Environmental Fluid Mechanics (2023) 23:1051–1073
https://doi.org/10.1007/s10652-022-09893-y

ORIGINAL ARTICLE

Entrainment dynamics of buoyant jets in a stably stratified environment

Partho Mukherjee[1] · Harish N. Mirajkar[2] · Sridhar Balasubramanian[1,3]

Received: 20 September 2021 / Accepted: 23 August 2022 / Published online: 4 September 2022

Abstract

Entrainment characteristics of a pure jet and buoyant jets in a stably-stratified ambient are compared with the help of laboratory experiments employing simultaneous particle image velocimetry and planar laser induced fluorescence techniques. For the buoyant jet, two cases of background stratification are considered, $N = 0.4\ \mathrm{s}^{-1}$ and $0.6\ \mathrm{s}^{-1}$, where N is the buoyancy frequency. Evolution of volume flux, Q, momentum flux, M, buoyancy flux, F, characteristic velocity, w_m, width, d_m, and buoyancy, b_m with axial distance is quantified that helps in understanding the mean flow characteristics. Subsequently, two different methods are used for computing the entrainment coefficient, α; namely the standard entrainment hypothesis based on the mass conservation equation and energy-consistent entrainment relation proposed by van Reeuwijk and Craske (J Fluid Mech 782:333–355, 2015). It is observed that entrainment coefficient is constant for the pure jet ($\alpha_{pj} \approx 0.1$) up until the point where the upper horizontal boundary starts to influence the flow. The entrainment coefficient for buoyant jets, α_{bj}, is not constant and varies with axial location before starting to detrain near the neutral layer. Near the source, $\alpha_{bj} \approx 0.12$ for both the values of N, while away from the source, $N = 0.6\ \mathrm{s}^{-1}$ exhibits a higher value of $\alpha_{bj} \approx 0.15$ in comparison to $\alpha_{bj} \approx 0.13$ for $N = 0.4\ \mathrm{s}^{-1}$. During detrainment near the neutral layer, $\alpha_{bj} \approx -0.2$ for $N = 0.4\ \mathrm{s}^{-1}$ and $\alpha_{bj} \approx -0.3$ for $N = 0.6\ \mathrm{s}^{-1}$. Importantly, close to the source, α from standard entrainment hypothesis and energy-consistent relation are in reasonable match for pure jet and buoyant jets. However, far away from the source, the energy-consistent relation is ineffective in quantifying the entrainment coefficient in the pure jet and detrainment in buoyant jets. We propose ways in which the energy-consistent relation could be reconciled with standard entrainment hypothesis in the far-field region.

Article Highlights

- Entrainment coefficient stays invariant for jets till the finite size of the domain in the axial direction disrupts this feature.
- Entrainment coefficient for buoyant jets evolving in a stratified ambient varies with axial distance followed by detrainment beyond the neutral layer.
- The existing entrainment relation performs reasonably well in the momentum dominated region but performs poorly when the finite size of the domain affects the flow for pure jet and when the flow is buoyancy dominated for the case of buoyant jets.

Extended author information available on the last page of the article

Keywords Buoyant jet · Momentum · Buoyancy · Entrainment · Detrainment

1 Introduction

A stream of fluid emanating from a point source driven purely by momentum and releasing into an ambient having the same density as the stream is called a pure or neutral jet. For this same stream of fluid, if its density (ρ_j) is different from that of the ambient (ρ_a), an additional force in the form of buoyancy influences the dynamics of the flow. The flow is termed as a positively buoyant jet (forced plume, $\rho_j < \rho_a$) or a negatively buoyant jet (fountain, $\rho_j > \rho_a$) depending on the densities of the ambient and the jet. If the flow is driven purely by buoyancy with no source momentum, it is known as a pure plume. A buoyant jet could also evolve in a stably-stratified environment making the flow more complex and rich in physics, whose characteristics are not well understood. All of these cases are commonly encountered in industrial and geophysical situations making it an important topic of research. The earliest work on jets revolved around characterising its mean flow behaviour, flow structure, instability, ensuing turbulence and entrainment characteristics [2–4] for tackling a variety of problems arising in mechanical and hydraulic engineering applications. Some early studies have also focused on the bulk flow and entrainment characteristics of buoyant jets and plumes in a stratified environment [5–7]. The authors were able to predict analytically (though approximate solutions) the mean velocity characteristics of the plume, the final height that it reaches, its entrainment characteristics or the degree to which it gets diluted and its spreading characteristics. The analytical expressions became essential tools in understanding and mitigating air and water pollution. Another important result was to distinguish whether a flow behaves more like a plume or a jet once it moved away from the source. A flux based parameter, $\Gamma \propto \frac{Q^2 F}{\alpha M^{\frac{5}{2}}}$ was defined by Morton [7] (a parameter comparing the ratio of buoyancy forces to inertial forces) that predicts whether the flow is purely momentum driven ($\Gamma \approx 0$, pure jet), purely buoyancy driven ($\Gamma \approx 1$, pure plume; $\Gamma > 1$, lazy plume), or driven by both momentum and buoyancy ($0 < \Gamma < 1$, buoyant jet or forced plume). Here Q is the volume flux, F is the buoyancy flux, M is the momentum flux at any axial location z from the source and α is the entrainment coefficient (mathematical form of all these quantities are shown later). The parameter Γ is analogous to the Richardson number (Ri) and represents the ratio of buoyancy flux to energy flux associated with momentum. The way in which it is constructed, it takes into account the energetics of the flow whereas Ri is purely the ratio between the two forces.

Wong and Wright [8] formulated a bifurcation parameter for linearly stratified ambient, $\sigma = \left(\frac{MN}{F}\right)^{0.75}$, where $N = \sqrt{-\frac{g}{\rho_0}\frac{d\rho_a(z)}{dz}}$ is the Brunt-V*ä*is*ä*l*ä* frequency, and is a static stability criterion for a stably-stratified ambient, $\rho_a(z)$ is the density of the ambient that is now varying with height, and ρ_0 is a reference density. With the help of experimental results, they concluded that if $\sigma < 1$, the flow exhibited pure plume like characteristics, if $\sigma > 2$ it showed pure jet like characteristics and if $1 \leq \sigma \leq 2$, it showed combined characteristics of plume and a jet, in other words, a buoyant jet. Entrainment describes the process of engulfment/mixing of the ambient with the mean flow and entrainment coefficient is a numerical representation of how well the mixing or entrainment is happening. Turner [9] proposed that for an axisymmetric release the entrainment process can be hypothesized as:

$$-(r_e u_{r_e}) = \alpha r_m w_m \tag{1}$$

which shows that the radial velocity (u_{r_e}) with which the ambient is engulfed in the jet/plume is proportional to its mean velocity, w_m and α, the entrainment coefficient is the proportionality constant. Here r_e is the radial location where the entrainment is happening and r_m is the radial extent of the jet/plume. Previous investigations have shown that the entrainment coefficient, α, for pure jet is a constant and for buoyant jet/pure plume, it is a function of the local Richardson number, $Ri(z)$ [5, 10, 11]. The various parameterizations available pointed to the fact that the α in a buoyant jet could be significantly different from a pure jet. Fischer et al. [12] proved this point further using experimental data and showed that buoyant jet diluted a lot faster and its α is higher than that of pure jet. Further complications arise when dealing with entrainment in positively buoyant jets in a stratified environment, especially when it reaches the neutral layer (height at which density of the buoyant jet becomes equal to the ambient density), a feature very similar to that of a fountain. Detrainment is a process through which a buoyant jet loses its fluid after reaching the neutral layer and its flow physics is hard to explain. As opposed to the entrainment process, where its velocity is always inwards towards the plume centre and one dimensional, detrainment velocity is two-dimensional in nature. The buoyant jet parcel not only moves radially outwards but also falls vertically downwards, which makes it difficult to quantify detrainment. However, looking at the variation of α with axial distance, a change in the sign is usually an indication of the detrainment process since the volume flux starts reducing after the neutral buoyant layer [13, 14].

Prior studies have shown that there could be significant variability in the α if different theoretical models are adopted for the same flow configuration. Priestley and Ball [5] used conservation equations for M, F and the mean kinetic energy E, while Morton et al. [6]) used the conservation equations for Q, M and F to study the bulk dynamics of buoyant jets and pure plumes evolving in uniform ($\rho_j \neq \rho_a$ and $N = 0\,\mathrm{s}^{-1}$) and stratified ambients. Apart from the mean flow governing equations, Telford [15] advocated for solving the turbulent kinetic energy (TKE) budget equation to be able to find the α in pure and buoyant jets more accurately. The argument was valid but the theoretical model could not be tested at that time because the turbulent fluctuating quantities are notoriously difficult to capture. With advent of laser-based techniques, it is now possible to find the mean and fluctuating velocity and density fields for a given plane over a period of time. Investigations by [16–19] quantified and showed the effect of turbulence in pure jet's and buoyant jet's evolution, tendency of buoyancy-driven turbulence to transport more tracer when compared to jet turbulence, clearly indicating that turbulence also affects the entrainment dynamics. Measurements of velocity and density fields using Particle Image Velocimetry (PIV) and Planar Laser Induced Fluorescence (PLIF), which are non intrusive in nature, provide more detailed localized measurements. Xu and Chen [20] studied the flow structure, mixing dynamics using TKE budget equation and visualized entrainment characteristics of a buoyant jet discharged horizontally into an ambient. Mirajkar et al. [21] studied positively buoyant jet and compared various characteristics with that of pure jet. It was seen that the decay of centerline velocity for the buoyant jet followed a power law, $W_c \propto z^{-a}$ but abruptly reduced to zero just above the neutral layer, while for pure jet it decreased indefinitely and followed a power law $W_c \propto z^{-1}$. Turbulence was also characterized, where several quantities of interest like the TKE, Reynolds stresses, turbulence intensity were reported. Overall, the results indicated that introducing buoyancy effects in the system can alter the mean flow and turbulence characteristics. More recently, Talluru et al. [22] through simultaneous PIV-PLIF, compared the evolution of a pure jet and a buoyant jet in a uniform ambient. They showed that the turbulence statistics do not scale with W_c for the latter, although the turbulence structures were quite similar for both. In recent times, the pursuit has been to characterize the entrainment dynamics of a buoyant jet in a stably-stratified ambient, i.e. $N > 0s^{-1}$, the understanding of which still remains obscured and thus it becomes the motivation behind this work.

In this experimental study, we use PIV to capture the velocity field of a pure jet and simultaneous PIV-PLIF to capture the velocity and density fields of a positively buoyant jet evolving in linear stably-stratified environments. Using the simultaneous velocity-density fields, the mean flow features such as evolution of volume flux, momentum flux, buoyancy flux, and characteristic velocity, width, buoyancy are found. Subsequently, entrainment coefficient is quantified using two methods: (a) by using the standard entrainment hypothesis and (b) by using the energy-consistent entrainment relation as proposed by van Reeuwijk and Craske [1]. The rest of the paper is structured as follows: In Sect. 2, the theoretical aspects of the problem are discussed, in Sect. 3, the experimental setup is explained, which is followed by results and discussions in Sect. 4. The paper is concluded in Sect. 5 with some key takeaways from our study.

2 Theoretical considerations

In this section the energy consistent entrainment relation as put forth by van Reeuwijk and Craske [1] is briefly discussed. At this point it will be useful to distinguish between an entrainment model and an entrainment relation. An entrainment model (for e.g. [5, 6]) usually takes into consideration a subset of the relevant mean flow governing equations to study either the near-field or far-field entrainment characteristics. On the other hand, an entrainment relation strives to provide a generalized solution by strategically identifying the important field variables that will contribute to the entrainment process and identifying the hierarchy in which all the relevant governing equations need to be solved. A model is at best a subset of a larger set of solutions generated by a universal entrainment relation. In this paper, we have chosen the entrainment relation put forth by van Reeuwijk and Craske [1], that appears quite robust and it been tested with the results available in literature for pure and buoyant jets in a uniform ambient. The entrainment relation has also been tested for more complex scenarios, such as, for the case where pure jet exit shape was varied by Breda and Buxton [23], for temporally evolving plumes by Krug et al. [24], and for an addition of an instantaneous body force in the form of volumetric heating in a jet by Pant and Bhattacharya [25]. Even in these cases, the study was either conducted on a pure jet or a buoyant jet in a uniform ambient, with minor additions to the simplified set of governing equations. In the present work, we try to extend the validity of the entrainment relation for a linearly stratified ambient focusing especially on the region above the height of neutral buoyancy for which the buoyant jet and ambient interact by way of detrainment. The important assumptions to solve the problem analytically are: the jet fluid and the ambient fluid are miscible, the flow is steady, incompressible, Bousinessq approximation is valid, viscous dissipation is neglected in the mean flow (since the flow is inherently turbulent, and it is a case of a free-shear flow), there is no exchange of heat between the jet and the ambient and it is chemically non-reactive. For a buoyant jet with a circular cross section, the integral form of the governing equations are:

$$\frac{dQ}{dz} = 2\alpha M^{\frac{1}{2}} \tag{2}$$

$$\frac{d}{dz}(\beta_g M) = B = \frac{FQ}{\theta_m M} \tag{3}$$

$$\frac{d}{dz}\left(\frac{\theta_g}{\theta_m}F\right) = -N^2 Q \tag{4}$$

$$\frac{d}{dz}\left(\gamma_g \frac{M^2}{Q}\right) = \delta_g \frac{M^{\frac{5}{2}}}{Q^2} + 2F \tag{5}$$

where β, θ, γ, δ are non-dimensional coefficients associated with momentum flux, buoyancy flux, energy flux and turbulence production respectively. The coefficients are distributed along the entire plume width as a function of the radial co-ordinate, r and these can be interpreted as shape functions or how the flux quantities are spread out across the plume width. The profile coefficients (e.g. β) are composed of both mean (β_m) and the fluctuating (β_f) components, and their algebraic sum is denoted by a gross value ($\beta_g = \beta_m + \beta_f$). The profile coefficients are given as:

$$\beta_m = \frac{M}{w_m^2 d_m^2} = 1, \quad \beta_f = \frac{2}{w_m^2 d_m^2}\int_0^\infty \overline{w'^2}\pi r dr \tag{6}$$

$$\gamma_m = \frac{2}{w_m^3 d_m^2}\int_0^\infty \overline{w}^3 \pi r dr, \quad \gamma_f = \frac{4}{w_m^3 d_m^2}\int_0^\infty \overline{w}\overline{w'^2}\pi r dr \tag{7}$$

$$\delta_m = \frac{4}{w_m^3 d_m}\int_0^\infty \overline{w'u'}\frac{d\overline{w}}{dr}\pi r dr, \quad \delta_f = \frac{4}{w_m^3 d_m}\int_0^\infty \overline{w'^2}\frac{d\overline{w}}{dz}\pi r dr \tag{8}$$

$$\theta_m = \frac{F}{w_m b_m d_m^2}, \quad \theta_f = \frac{2}{w_m b_m d_m^2}\int_0^\infty \overline{w'b'}\pi r dr \tag{9}$$

where characteristic velocity (w_m), characteristic width (d_m), characteristic buoyancy (b_m) and a plume Richardson number (Ri) are in the following form:

$$w_m = \frac{M}{Q} \quad d_m = \frac{Q}{M^{\frac{1}{2}}} \quad b_m = \frac{BM}{Q^2} \quad Ri = \frac{BQ}{M^{\frac{3}{2}}} \tag{10}$$

The volume flux (Q), momentum flux (M), integral buoyancy (B) and buoyancy flux (F) are written as:

$$Q = 2\int_0^\infty \overline{w}\pi r dr \quad M = 2\int_0^\infty \overline{w}^2 \pi r dr \quad B = 2\int_0^\infty \overline{b}\pi r dr \quad F = 2\int_0^\infty \overline{b}\overline{w}\pi r dr \tag{11}$$

Here w is the velocity in the axial (z) direction. The net body force in the form of reduced gravity or buoyancy is denoted by $b = g\frac{\rho_a - \rho}{\rho_o}$, and $\overline{(\cdot)}$ indicates that these quantities are time-averaged and $(\cdot)'$ is the fluctuation of the field variable around its time average.

Equations 2–5 are the final form of the governing equations (conservation of mass, momentum, buoyancy flux and energy) used to find the entrainment relation. A point worth mentioning here is that in Eq. 3, integral buoyancy, B is expressed in terms of buoyancy flux F, so that the momentum equation itself embodies the buoyancy flux term. This simplification was made in van Reeuwijk and Craske [1] because the theoretical relation proposed by them was for a case when the ambient is uniform ($N = 0$). That makes Eq. 4 redundant, because the right hand side is zero and therefore F is a constant. Thus, only three governing equations have to be solved, viz. Eqs. 2, 3 and 5 that has three unknowns Q, M and F. In the current study, although $N \neq 0$, it is worth exploring how the existing entrainment relation performs in such cases, which has not been done in the past. As we will see later, it performs reasonably well for region close to the source and poorly in the region far from the source. Another point worth mentioning is that in van Reeuwijk and Craske [1], the profile coefficients in addition to mean and fluctuating components also had contribution from the pressure field, its fluctuation and its gradient. Since it is impossible in the present experimental case to measure the pressure field, we have omitted its contribution. We also believe that because the flow and the fluid that is used in the present case are incompressible, the effect of pressure on the entrainment dynamics should be negligible. As we will see later, the theoretical relation even without the contribution from the pressure field still yields satisfactory results. Finally, using the above equations, the entrainment relation is given by Eq. 12b:

$$\alpha = \frac{1}{2M^{\frac{1}{2}}}\frac{dQ}{dz} \tag{12a}$$

$$= -\frac{\delta_g}{2\gamma_g} + \left(\frac{1}{\beta_g} - \frac{\theta_m}{\gamma_g}\right)Ri + \frac{Q}{2M^{\frac{1}{2}}}\frac{d}{dz}\left(log_e\frac{\gamma_g}{\beta_g^2}\right) \tag{12b}$$

Prior to [1, 26] also explored this idea and explained the physical mechanism of the three different terms in Eq. 12b, the only difference being that the contribution from the fluctuating field was not considered in their case. Equation 12a is merely a rearrangement of Eq. 2, and the entrainment can directly be quantified using this expression. Equation 12b or the entrainment relation is obtained after a few mathematical manipulations of Eq. 12a (by expanding and expressing the volume conservation equation by invoking the momentum and energy equations) and it quantifies the individual mechanisms that contribute to α. Ideally, a good match should be obtained for α when comparing Eq. 12b with the standard entrainment hypothesis, viz., Eq. 12a; something that is explored in this study.

There are three different mechanisms that contribute to the entrainment relation. First one ($-\frac{\delta_g}{2\gamma_g}$), is the ratio of the gross profile coefficients of turbulence production and mean kinetic energy, which indicates the fraction of mean kinetic energy being converted to turbulent kinetic energy production that aids in entrainment. The second term, $\left(\frac{1}{\beta_g} - \frac{\theta_m}{\gamma_g}\right)Ri$ is the representation of buoyancy force, which indicates entrainment (positive value) or detrainment (negative value). Lastly, the third term, $\frac{Q}{2M^{\frac{1}{2}}}\frac{d}{dz}\left(log_e\frac{\gamma_g}{\beta_g^2}\right)$ represents how the departure from self-similarity influences α. If the third term is zero, it would mean that self-similarity is attained and there is no further contribution from it. If this term is negative, that will indicate a break in self-similarity and lowering of α. While a positive value indicates that the jet/plume is in the process of attaining self-similarity, thereby increasing α.

The motive behind the current work is to first quantify α for pure jet and buoyant jets evolving in a linear stably stratified ambient through standard entrainment hypothesis (SEH, Eq. 12a). Following this, α is quantified using the energy-consistent entrainment relation (ER) by computing all the individual terms appearing in Eq. 12b. Lastly, the entrainment coefficients obtained by these two methods are compared and conclusions are drawn. The novelty of this work lies in the fact that α has not been quantified for a buoyant jet evolving in a linearly stratified ambient and a comparative study for α using SEH and ER has also not been reported. Therefore, the results from this study would provide a baseline value for α while also quantifying the role of various mechanisms that contribute to its evolution.

3 Experimental setup and flow conditions

The setup consists of two acrylic tanks, T1 (60 cm × 60 cm × 60 cm) and T2 (91 cm × 91 cm × 60 cm) and a double bucket system (B1 and B2) as shown in Fig. 1. The jet fluid is stored in T1 and the linearly stratified ambient fluid created using a double-bucket system is kept in T2. A linear stable stratification is achieved by using a combination of commercial salt, isopropyl alcohol and water. The bucket B1 holds the mixture of water and isoproyl alcohol and the bucket B2 holds the mixture of water and commercial salt. Initially the level of the fluid in both the buckets are maintained in a manner such that the pressure at the bottom of both the buckets are the same and opening the control valve, CV1 will not cause any fluid motion. The ambient stratification in tank T2 builds up once the control valves, CV2 and CV1 are simultaneously opened [27]. A stirrer is provided in B2 that mixes the incoming lighter fluid from B1 and the heavier fluid (in B2) constantly, so that the fluid in the tank remains homogenised and the density of the fluid released by CV2 is continuously reducing as a smooth function of time. A centrifugal pump is used to transport the jet fluid from T1 to T2 with the help of a nozzle having a diameter, D = 12.7 mm. A control valve is placed to regulate the flow rate, which is quantified using an

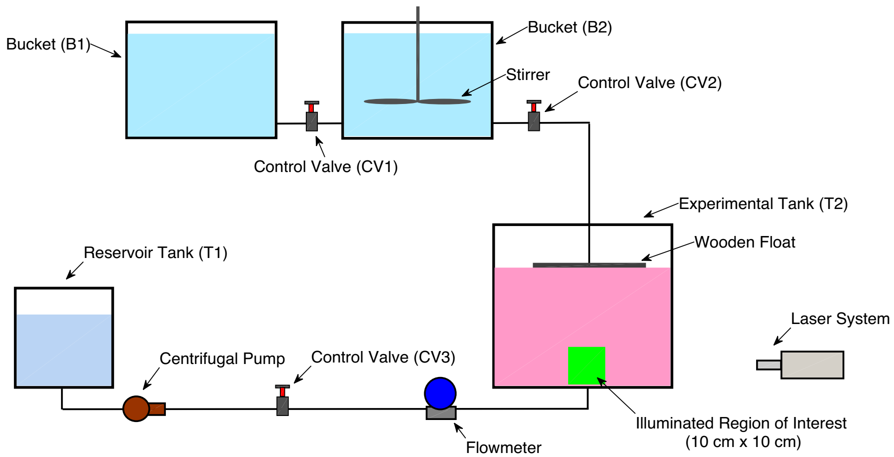

Fig. 1 Schematic of the experimental setup. The cameras are positioned in a manner such that the illuminated region is viewed in the way the reader is viewing it

electromagnetic flow-meter. Three individual cases are considered for our study: (a) pure jet, (b) positively buoyant jet A ($N = 0.4\,\mathrm{s}^{-1}$) henceforth referred to as BJA, and (c) positively buoyant jet B ($N = 0.6\,\mathrm{s}^{-1}$), henceforth referred to as BJB. The source Reynolds number, Re_o, is maintained as $Re_o \approx 3100$ for all the experiments based on the density of jet (ρ_j), average velocity ($W_o = 0.22$ ms^{-1}), source diameter (D) and dynamic viscosity ($\mu \approx 9 \times 10^{-4}$ Pa.s). The details of important source parameters are given in Table 1.

The plume fluid from the reservoir tank is injected into the experimental tank using a round jet nozzle and a centrifugal pump. The nozzle is designed based on the design concept of a wind tunnel [28], and is built in house using electrical discharge machining technique. It is made of aluminium, having a length of 160 mm and an exit diameter $D = 12.7$ mm, and consists of a diffuser, settling chamber, and a contraction section. The diffuser has an expansion section first with a gradually changing profile, which aids in reducing the flow turbulent fluctuations. In the diffuser section, the velocity reduces and the pressure imparts the necessary momentum to keep the fluid moving in the downstream location. After the expansion section, the nozzle has a constant cross-section called the settling chamber, followed by a contraction section to reduce the development of a boundary layer. A honeycomb is placed in the settling chamber to further reduce the small-scale fluctuations and generate an uniform flow at the nozzle exit. This provided a conditioned flow with minimum fluctuations.

Particle image velocimetry (PIV) is used to capture $2-D$ velocity field in the radial (r) and vertical or axial (z) directions at every instance of time. A 1 mm thin rectangular sheet of Nd:YAG pulse laser (532 nm, 145 mJ/pulse) is first aligned parallel to the front wall of the tank T2 so that the measurements are made precisely in a $r-z$ plane. The laser sheet's position is further adjusted such that the centerline of the jet lies in the illuminated plane. Since two different fluids, i.e., brine and isopropyl alcohol are used, the refractive indices are carefully matched to avoid any optical aberrations. Polyamide particles with mean diameter 55 μm and specific gravity 1.03 are used to keep track of the fluid flow. The size and the density of the particle are chosen in a manner such that it remains suspended (neutrally buoyant) in the ambient for a long period of time. This ensures that the particles remain passive with the flow and captures the dynamics effectively. Both ambient and jet fluids are seeded to obtain PIV images with well-distributed particles, which ensures high signal to noise ratio during post processing. To obtain mean and turbulence statistics from PIV, it is important to have a high spatial resolution that has the ability to resolve the Kolmogorov length-scale. In connection with the present work, the high spatial resolution helps in resolving the flux quantities and its derivatives used for quantifying the entrainment coefficient in (Eq. 12a) and the profile coefficients and its ratios and derivatives in (Eq. 12b), whose accuracy once again depends on how well the Kolmogorov length scale is resolved. The ratio of the PIV vector resolution and the Kolmogorov length scale in the present work is $\frac{\Delta_{PIV}}{L_\kappa} \leq 3$ and it gives fairly good results. In order to achieve this, entire jet/buoyant jet region is divided into four different layers (based on the maximum height attained). The dynamics of each layer is obtained by conducting four different experiments. The uncertainties associated with this procedure is minimised by using sufficient number of images, providing an overlap while transitioning from one layer to the other and by conducting experiments for each of the layer at least three times. Utmost care was exercised to ensure that stratification strength, N, remained same during the individual runs (within $\pm 1\%$). The time interval, Δt, between the two pulses was also varied in these individual runs for the same experiment to account for the fact that the jet slows down as it moves vertically away from the source. For each experimental run, at least 1000 images were recorded for both velocity and density fields and 600 of them were used for the analysis to reduce the statistical random error and for convergence (see [29]). The density field is obtained using PLIF for the same window and using a separate camera. The laser source for both PIV and PLIF is the same. Rhodamine 6G (R6G) is used as a fluorescent dye that is mixed uniformly with the ambient fluid (only). The camera is equipped with an appropriate filter to record only the R6G signal. The R6G concentrations in ambient and jet fluids are 100 μg L^{-1} and 0 μg L^{-1} respectively. The gray value of the image and the R6G concentration are calibrated first by varying the concentration of R6G. Decoding the image gray value, it is observed that R6G concentration is linearly proportional to the local density field. So when the two fluids mix, the local concentration of R6G in that region changes, and so does the local fluid density that could be expressed as:

$$\rho = \rho_j - \frac{C}{C_1}\left[\rho_j - \rho_a\right] \tag{13}$$

where C is the intensity of the evolving jet, C_1 is the intensity of the background medium, which also takes care of its laser intensity absorption factor. The quantified form of instantaneous fields were obtained after processing the raw images and subsequently MATLAB was used for analysis of the data to obtain the desired results.

The common sources of PIV uncertainty are due to the limitations in the temporal and spatial resolutions and any interpolation or smoothing of vectors. The spatial resolution for both PIV and PLIF is ≈ 855 μm/pixel and knowing that the uncertainty in the location of a particle is half the pixel size, we estimate the error in the velocity measurements to be ≈ ±6%. The error related with temporal resolution is minor and averaging over a large number of ensembles significantly reduces it. Finally the uncertainty associated with interpolation of vectors is quite low inside the jet region (±3%) and slightly higher (±5%) near the edge. The primary source of error in PLIF comes from calibration and laser intensity attenuation. The error due to light absorption on the measured peak intensity was calculated to be less than ≈ ±2%. The error in the instantaneous density measurements due to calibration was estimated to be ≈ ±3.5%. All the uncertainties mentioned are well within the experimental uncertainty range.

4 Results and discussions

4.1 Qualitative analysis

In this sub-section, the entrainment characteristics are discussed qualitatively with the help of radial velocity contour maps. In a linearly stratified ambient, the buoyant jet reaches a maximum height, Z_m, before starting to spread radially [30]. The maximum height for BJA ($N = 0.4s^{-1}$) is $Z_m = 32$ cm and for BJB ($N = 0.6\,\mathrm{s}^{-1}$) is $Z_m = 27.5$ cm. The neutral layer is at an axial distance of $z/D \approx 16$ and $z/D \approx 14$ from the source respectively. Based on the entrainment features and jet properties, the entire axial span is divided into three zones. For buoyant jets, zone one is the region from the source till the Morton length scale (l_m). Zone two is the region spanning from the l_m till the neutral buoyancy level and zone three is the region above the neutral buoyancy level. For the pure jet case, zone one and two is the region where α is nearly constant ($z/D < 20$) and zone three is where the α drops significantly.

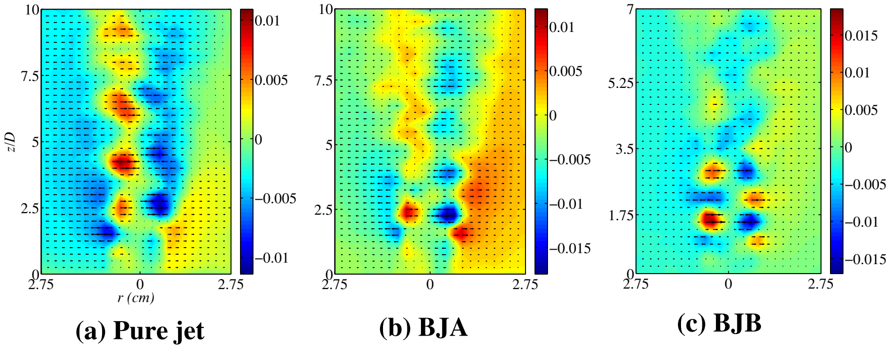

Fig. 2 Radial velocity (in ms^{-1}) contour maps for pure jet, buoyant jet A and B in zone one

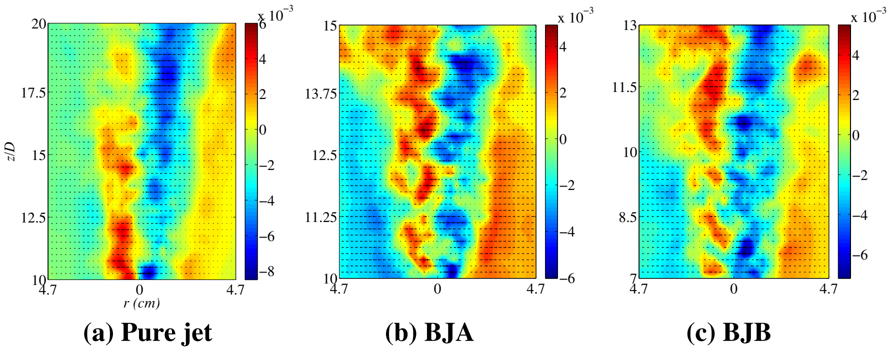

Fig. 3 Radial velocity (in ms^{-1}) contour maps for pure jet, buoyant jet A and B in zone two

In Fig. 2, the radial velocities in zone one for pure jet, BJA, and BJB are presented and in all the cases the entrainment is somewhat patchy. The positive and negative values, both of which indicate a radially inward flow, show, that as pure and buoyant jets move axially away from the source, entrainment happens intermittently in patches. Another feature common in all the three cases in zone one is the presence of a very small region ($0 < z/D < 2$) where the flow is radially outward near the source. This anomalous behaviour is most certainly because of the presence of small-size eddies or starting vortex because of high velocity gradients and a change in the shape of velocity profiles which indicates development region. Overall, the entrainment characteristics are similar in zone one for pure jet, BJA, and BJB. Moving to zone two (see Fig. 3), the entrainment is more continuous in nature, with BJA and BJB having a larger engulfing region due to the presence of buoyancy force. Finally in zone three, the entrainment characteristics are completely different for pure and buoyant jets. For pure jet, weak entrainment continues to happen (see Fig. 4a). On the other hand, for BJA and BJB, negative buoyancy force starts to dominate the flow momentum. As the buoyant jet penetrates the neutral layer (see Fig. 4b, c), there is a reversal of direction in the radial velocity, and it is now pointing outward, indicating the detrainment process, which is absent in the case of pure jet.

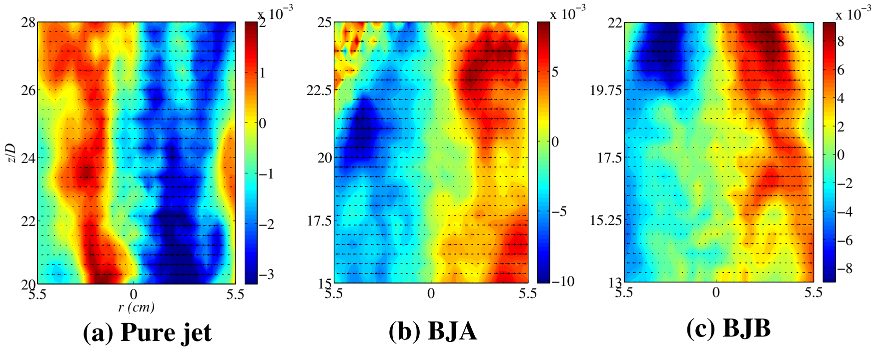

Fig. 4 Radial velocity (in ms^{-1}) contour maps for pure jet, buoyant jet A and B in zone three

4.2 Mean flow parameters and derived quantities

In this sub-section, the dynamics of pure and buoyant jets based on important flux parameters are discussed, which helps in understanding the influence of source parameters on their evolution. Before we begin, the manner in which the relevant quantities in this study are computed are discussed. At first, the flux quantities in Eq. 11 are computed, for which we need to find the mean axial velocity, $\overline{w}$, and mean density, $\overline{\rho}$. A total of $N_t = 600$ images (120 seconds) are used to find the mean velocity and density fields, which could be represented as:

$$\overline{w} = \frac{1}{N_t}\sum_{1}^{N_t} w \qquad \overline{\rho} = \frac{1}{N_t}\sum_{1}^{N_t} \rho \tag{14}$$

Following this, the quantities are integrated over the jet width (Eq. 11) for each axial location, z, to find the variation of the flux quantities as a function of z. The integration process uses a continuous function as an integrand, but in the experiments we only have a set of data points that is discrete. The summation process in this case can be represented as:

$$X = 2\sum_{0}^{r_0} \overline{f}\,\pi\, r^*\,\Delta r \tag{15}$$

where X is any given flux parameter (Q, M, B, F) and $\overline{f}$ is a mean field variable ($\overline{w}$ or $\overline{\rho}$) at a particular radial location r^*, Δr is the distance between two consecutive radial locations, which is close to 1 mm, and r_0 is the location where $\overline{w}/W_c \approx 0.05$. The flux parameters are then used to find the derived quantities (w_m, d_m, b_m, Ri). The resolution used in the experiments is sufficiently small such that the discrete summation process is practically the same as integration. This argument is verified by computing the flux parameters using this summation process at an axial location near the jet exit, which turns out to be very close to their respective source values as shown in Table 1. Subsequently, the profile coefficients in Eqs. 6–9 are computed using a similar summation process, only difference being that the integrands now also contain the fluctuating component of the field variables.

In Fig. 5, the variation of volume flux as a function of axial distance is shown. All the three experimental cases (pure jet, BJA, and BJB) are shown in the same figure so that the differences could be clearly observed. It is seen here that for pure jet the volume flux Q,

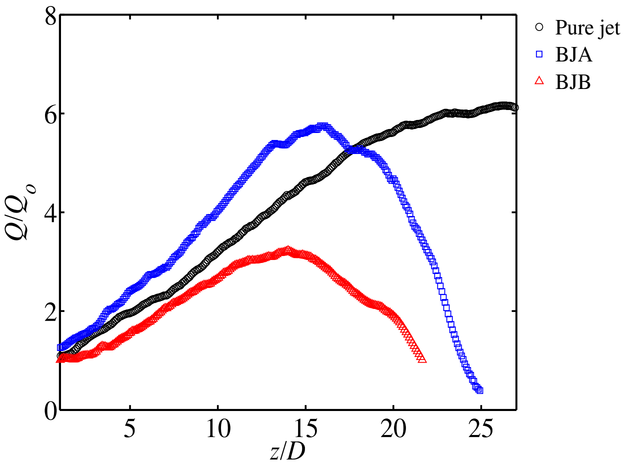

Fig. 5 Variation of normalised volume flux with normalised axial distance for pure jet, buoyant jet A and B. Details of all the source values used for normalizing are provided in Table 1

increases monotonically with axial distance due to continuous entrainment of ambient fluid. In conjunction with Figs. 6 and 7, which show the variation of characteristic velocity w_m and width d_m, we conclude that although w_m decays for pure jet, Q keeps increasing as a result of entrainment that increases d_m. Therefore, increase in Q compared to its source value Q_o is a representation of the entrainment process. Next we look into the variation of Q for BJA ($N = 0.4\,\mathrm{s}^{-1}$) and BJB ($N = 0.6\,\mathrm{s}^{-1}$), which is also shown in Fig. 5. Some interesting qualitative and quantitative differences could be seen in comparison with pure jet. In a linearly stratified environment, the jet engulfs the ambient fluid in a monotonic manner upto the neutral layer. Beyond the neutral layer, the volume flux rapidly reduces indicating entrainment loss or detrainment. Now, if Q_o, M_o and Re_o are held constant, the height of the neutral layer is inversely proportional to the stratification strength (as shown in [30]). This

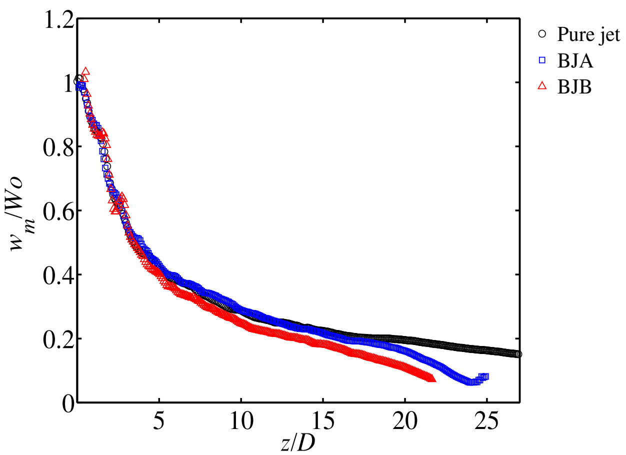

Fig. 6 Variation of normalised characteristic velocity with normalised axial distance for pure jet, buoyant jet A and B

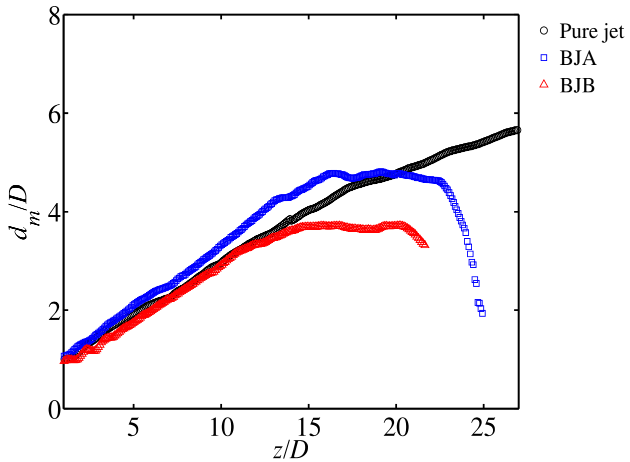

Fig. 7 Variation of normalised characteristic width with normalised axial distance for pure jet, buoyant jet A and B

feature is distinctly seen in Fig. 5, wherein, the Q peaks and starts to reduce for BJB ($N = 0.6\,\mathrm{s}^{-1}$) much earlier, at $z/D \approx 14$, than BJA ($N = 0.4\,\mathrm{s}^{-1}$), where Q peaks at $z/D \approx 16$. The Q of pure jet is consistently lower than that of BJA upto the neutral layer height. This indicates that introducing buoyancy effects in the system increases the quantity of the ambient fluid that is engulfed in the mean flow. On the other hand, the volume flux is consistently lower for BJB ($N = 0.6s^{-1}$), despite stratification strength being higher. Before the detrainment process begins at the neutral layer, $\frac{Q}{Q_0} \approx 6$ for BJA ($N = 0.4\,\mathrm{s}^{-1}$), whereas, for BJB ($N = 0.6s^{-1}$), $\frac{Q}{Q_0} \approx 3$ at the neutral layer. This shows that the bifurcation parameter σ plays an important role in determining the amount of ambient fluid that is engulfed. Thus, at a particular axial distance from the source, $\frac{Q}{Q_0}$ varies non-monotonically with σ, which is confirmed through multiple experimental runs. Finally, pure jet does not see any detrainment due to the absence of a neutral layer. It is able to engulf almost six times the source volume flux but at a much farther axial distance ($z/D \approx 20$) from the source before reaching a plateau because of the influence of the upper horizontal boundary.

Invoking w_m and d_m, shown in Figs. 6 and 7 respectively, adds more physics-based explanation as to why Q is different for buoyant and pure jets. It also helps explain the lower Q for BJB compared to BJA and pure jet. As discussed earlier, w_m decreases and d_m increases in a monotonic manner for a pure jet. However, w_m for BJA & BJB decay at a faster rate and abruptly reaches zero once it crosses the neutral layer (i.e., at its maximum height, Z_m). Likewise, d_m increases but abruptly drops once the buoyant jet reaches the neutral layer. From the same figure, it is also seen that at a particular z/D location, d_m is different for pure and buoyant jets. This indicates that σ influences the lateral spreading of buoyant jets and BJA has a slightly higher lateral spread as compared to BJB. This is also consistent with the amount of fluid (Q) that BJA and BJB entrains, as discussed previously. Near the source though ($z/D < 4$), w_m and d_m seems to be independent of the source parameters as the decay rate and spread rate seems to be the same for pure and buoyant jets. This indicates that buoyant jets have pure jet like characteristics in the momentum dominated region, within the Morton length-scale, l_m. When the buoyancy force becomes more dominant, typically beyond l_m, the difference between the behaviour of pure and buoyant jets becomes distinct. It should be pointed out that w_m and d_m in this study are found based on the evolution of Q and M (see Eq. 10) and therefore a function of the width of the velocity profiles. If the plume-width is based on a scalar or density field, it may differ from the present study. Some of these features along with turbulence characteristics for pure and negatively buoyant jets in uniform ambient are also discussed in [22].

In Fig. 8, the variation of momentum flux M with axial distance is shown for all the three cases. Referring to Eq. 3, it is seen that the momentum of the flow remains unaltered for a pure jet. This assumption holds true from a practical standpoint up until $z/D \approx 20$ for the pure jet case. Beyond this region, the upper horizontal boundary starts to influence the flow dynamics. For the case of buoyant jet, the momentum will increase with axial distance due to the presence of a body force in the form of positive buoyancy. In a stratified ambient, beyond the neutral the negative buoyancy force takes over and the momentum of the flow decreases, this is discussed further in sec. 4.4. In both pure and buoyant jets, the zone close to the source ($z/D < 4$) is where the velocity profiles develop from top-hat to Gaussian. This is also the region of laminar-turbulence transition and a sharp drop in M is observed (see Fig. 8) in all the three experimental cases. Presently, our conjecture is that the sudden drop in M at the exit of the nozzle is because of the initial adjustments that the flow makes to counter the weight of the ambient. Later, as the pure jet/buoyant jet evolves in space, there is a marginal increase in the momentum indicating a recovery. Several experimental runs have been performed that confirm the existence of this phenomenon. At present, for the pure jet case, the study of this anomalous behaviour of momentum recovery is beyond the scope of this study.

As we move away from the source, M for the pure jet recovers almost to its source value and then drops beyond $z/D > 20$ because of the presence of upper horizontal boundary. For the case of a buoyant jet, the role of buoyancy force and stratification strength on the flow dynamics is evident from Figs. 8 and 9. Positive buoyancy force aids the momentum of the flow (see Eq. 3), whereas stratification strength via. the buoyancy flux conservation

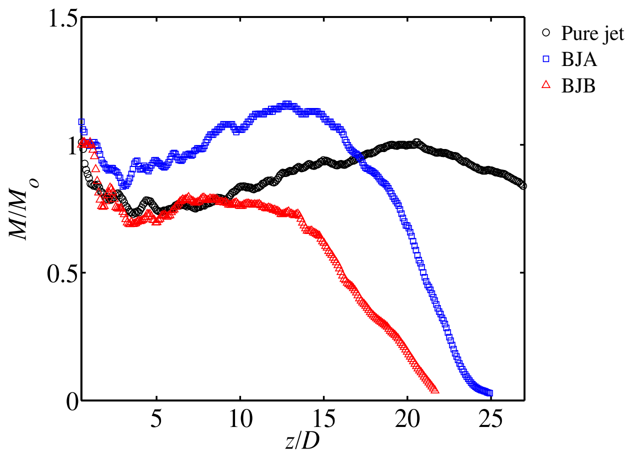

Fig. 8 Variation of normalised momentum flux with normalised axial distance for pure jet, buoyant jet A and B

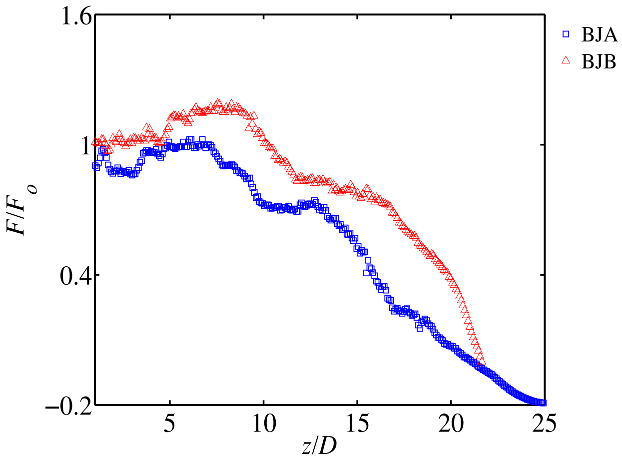

Fig. 9 Variation of normalised buoyancy flux with normalised axial distance for buoyant jet A and B

equation (see Eq. 4) influences the kinetic energy of the flow. This becomes clear when the evolution of M is compared for BJA ($N = 0.4\,s^{-1}$) and BJB ($N = 0.6\,s^{-1}$) in Fig. 8. Higher stratification leads to more dilution of the buoyant jet fluid, the positive buoyancy effects are quickly negated and therefore M of BJB is consistently lower compared to BJA. As the buoyant jet reaches the neutral layer signified by $B/B_o \approx 0$, M starts to decrease. The neutral buoyancy level also forces the buoyant jet to lose its fluid (i.e. detrainment) causing Q to go down. The results indicate that Figs. 5-9 are consistent with Eqs. 2–4. By discussing the results along with the governing equations, the importance of buoyancy and stratification strength in the evolution of buoyant jet and the entrainment/detrainment process becomes clear. Figure 10 presents the characteristic buoyancy b_m as a function of z. As the buoyant jet entrains with the ambient, it gets diluted and therefore b_m keeps reducing with axial distance. Finally, b_m drops below zero beyond the neutral layer during the detrainment process and the residual momentum and buoyancy in this region is advected away in the radial direction.

4.3 Entrainment characteristics of pure and buoyant jets

The entrainment coefficient, α, is found using the standard entrainment hypothesis (Eq. 12a) and using the entrainment relation (Eq. 12b). The entrainment relation quantifies the individual mechanisms that contribute to the entrainment process. The algebraic sum of all the contributors should be equal to α obtained the using standard entrainment hypothesis. In previous literature, for a pure jet, α has been found to be around 0.1 ± 0.02, whereas when there are buoyancy effects present, the α values can range from 0.09 - 0.3, and depends on Ri as documented in [31]. As we will see, the α values obtained in our study lies within these limits, except for the region far away from the source (represented by zone three in our study).

In Fig. 11, the variation of α with axial distance is shown for the case of a pure jet (α_{pj}) using Eq. 12a and b. This figure should be looked at in conjunction with Fig. 12 where the individual contributions to α_{pj} from the terms appearing in Eq. 12b are presented. Since, a pure jet is devoid of any buoyancy effects, α_{pj} does not change with z and assumes an

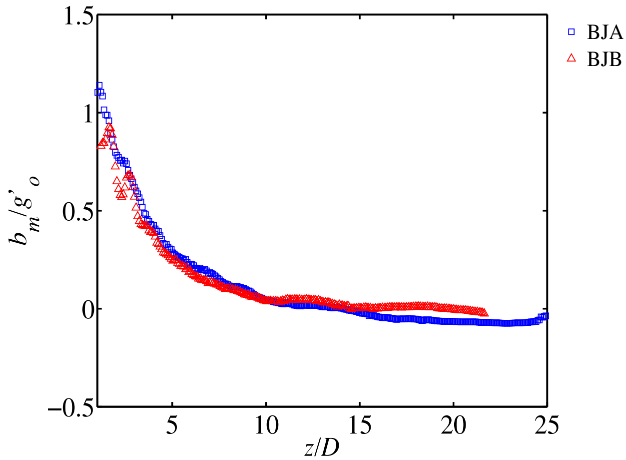

Fig. 10 Variation of normalised characteristic buoyancy with normalised axial distance for buoyant jet A and B

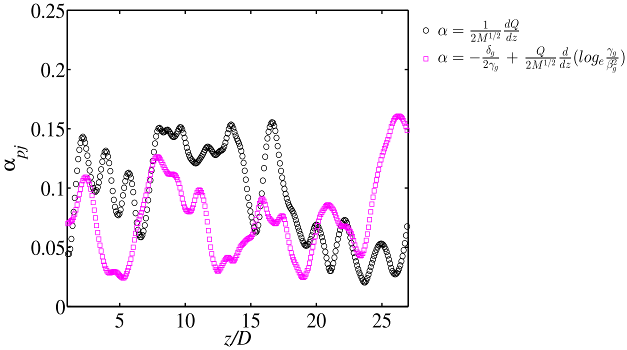

Fig. 11 Comparison of entrainment coefficient found using entrainment hypothesis and entrainment relation (Eq. 12a vs b) as a function of axial distance for pure jet

average value of $\alpha_{pj} \approx 0.095$-$0.098$ when the standard entrainment hypothesis is used in Fig. 11. Likewise, using the entrainment relation, α is estimated to be $\alpha_{pj} \approx 0.081$-$0.083$, until $z/D \approx 20$. Note that α_{pj} shows some oscillation around a mean value, which is inevitable in experiments due to measurement uncertainties and the fact that the entrainment is expressed as first derivative of flux quantities and profile coefficients (and its ratios) which is very sensitive to spatial resolution. Therefore, it is prudent to look at a spatially averaged value of α_{pj} from experimental measurements. Most importantly, up to $z/D \approx 20$, α_{pj} is nearly the same using 12a and 12b (see Table 2), which shows that α obtained using the entrainment relation agrees reasonably well with the standard entrainment hypothesis for the case of pure jet.

For $z/D > 20$, the entrainment relation (Eq. 12b) predicts a higher value, $\alpha_{pj} \approx 0.091$ compared to that obtained from standard entrainment hypothesis $\alpha_{pj} \approx 0.031$. This corresponds to the axial location where Q starts to plateau (see Fig. 5) for the pure jet case (pointing to a very low value of α) and M starts to dip (see Fig. 8). The inability of the

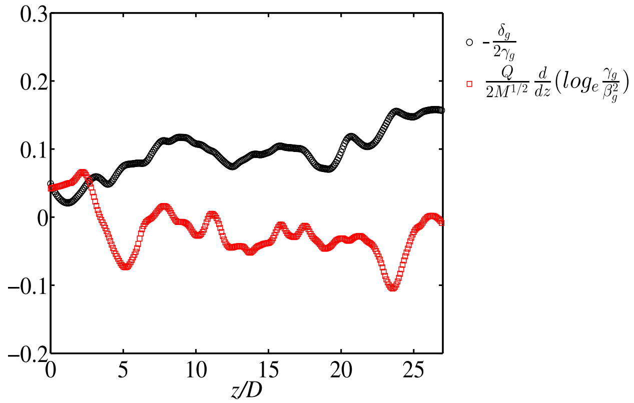

Fig. 12 Contributions from the different terms appearing in entrainment relation (Eq. 12b) for pure jet as a function of axial distance. The entrainment coefficient is the algebraic sum of all the terms

entrainment relation to match standard entrainment hypothesis in this zone points out that the there is an influence of opposite horizontal boundary that alters the turbulent nature of the jet, because of which its energy conserving nature breaks down. Theoretically, jets are energy conserving and self-similar, and therefore $\frac{dM}{dz} = 0$ (from Eq. 3) and M is a constant along the axial distance. Therefore, the Q should increase monotonically in a linear fashion (since, $\frac{dQ}{dz} \propto M$) with increasing axial distance (evident from Fig. 5). This poses a restriction that $\frac{dQ}{dz}$ is a constant and thus the proportionality constant α stays invariant for a pure jet, via. Eq. 12a. From a theoretical viewpoint, in the entrainment relation for a pure jet, only the energy conversion term (first term in Eq. 12b) would be non-zero. The similarity drift term (last term in Eq. 12b) should vanish because of the self-similar nature and the buoyancy term (second term in Eq. 12b) is zero because $Ri = 0$. However, in our experiments, a non-zero value of similarity drift term is seen in Fig. 12, which is expected from a practical standpoint. Despite this, the entrainment relation works reasonably well for the pure jet case up until $z/D \approx 20$. For the clarity of discussion, we classify the entire axial distance into three zones as shown in Table 2. The α for the pure jet case stays constant in zone one and two with a value of $\alpha_{pj} \approx$ 0.095-0.098. However, in zone three, α_{pj} value drops significantly to 0.031.

Figures 13 and 14 present α_{bj} found using the standard entrainment hypothesis for BJA ($N = 0.4\,\mathrm{s}^{-1}$) and BJB ($N = 0.6\,\mathrm{s}^{-1}$). The influence of Ri on the entrainment process can be clearly seen, as α_{bj} varies with axial distance, indicating it is a function of local Ri or $Ri(z)$. Zone one is the near-field region, where the buoyancy force is less dominant and the buoyant jet exhibits pure jet like characteristics. It is seen that the α found using standard entrainment hypothesis oscillates around a value of approximately 0.12 for both the cases of buoyant jet in zone one. Zone one for the BJA & BJB roughly turns out to be their respective Morton length-scale l_m that demarcates momentum dominated and buoyancy dominated regions. On the other hand, in zone two, the α for BJA & BJB starts to diverge. It is higher for BJB (0.15) than BJA (0.13), because of the difference in the buoyancy force and buoyancy flux and its influence on the momentum and energy equations. Zone two distinguishes the entrainment characteristics between pure and buoyant jets with clarity and emphasises the importance of buoyancy (indirectly the Ri) in the process of entrainment. Now, if Fig. 5 is also brought into the discussion, it can be seen that though BJB

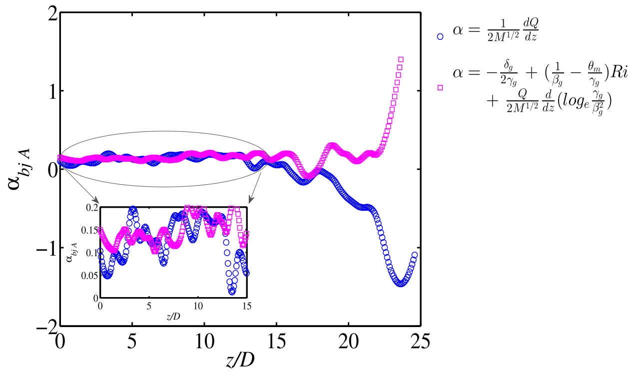

Fig. 13 Comparison of entrainment coefficient found using entrainment hypothesis and entrainment relation (Eq. 12a vs b) as a function of axial distance for buoyant jet A

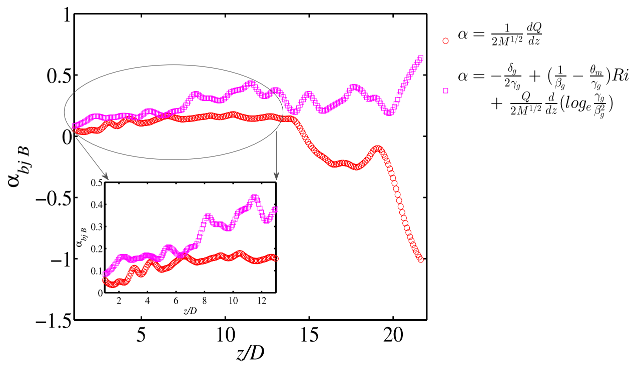

Fig. 14 Comparison of entrainment coefficient found using entrainment hypothesis and entrainment relation (Eq. 12a vs b) as a function of axial distance for buoyant jet B

($N = 0.6\,\mathrm{s}^{-1}$) has a higher α, the amount of fluid that it entrains is less compared to BJA ($N = 0.4s^{-1}$), since its Q is lower. This signifies that higher density difference between the buoyant jet and the ambient creates conditions for better mixing/entrainment (higher α) but σ controls the amount of fluid participating in the entrainment process. Zone three is the region around the neutral layer where the buoyant jet intrudes into the ambient indicating a detrainment process. The detrainment value of BJB is much higher ($\alpha_{bj} = -0.3$) compared to BJA ($\alpha_{bj} = -0.2$). Since, the plume fluid in BJB interacts with a much steeper stratification, stronger unstable motions exist above the neutral layer, thereby resulting in a higher detrainment.

Lastly, α_{bj} for BJA and BJB is quantified using the entrainment relation (Eq. 12b) and presented in Figs. 13 and 14. It is seen that the relation predicts a slightly higher value of α_{bj} in zone one and two (see Table 2). The qualitative trend is captured but the quantitative values differ. In zone three, we see that the entrainment relation does not comply with the experimental observations. The α_{bj} values in this region for BJA and BJB continues to be positive (well over 0.2) and the relation is unable to capture the detrainment process even qualitatively. The reasons for such discrepancies are discussed in the next sub-section.

4.4 Further discussions

In this sub-section, the discrepancies in the values of α found using the entrainment hypothesis (SEH) and the entrainment relation (ER) are discussed. We also discuss possible ways to reconcile the two approaches.

4.4.1 Zone one and two

Firstly, in the case of pure jet, it is seen that the disagreement between the two approaches remained well within the acceptable limits ($\approx 10-15\%$) in zone one and two. The theoretical formulation and experimental results match quite well in this case. For buoyant jets, the disagreement between the two approaches is somewhat higher but within $\approx 20\%$ in zone one but in zone two, the entrainment relation consistently predicts a higher α and considerable deviations are noticed. The minor deviations in zone one are probably because of the difficulty in capturing the fluctuating field variables very close to the source $(z/D < 4)$ for both pure and buoyant jets. The laminar-turbulence transition, zone of developing velocity profiles near the source are possible reasons behind it. This tiny region close to the source demands a better treatment, and it is beyond the scope of the current work and remains an open problem.

The major deviations in zone two in the case of buoyant jets may have two plausible reasons to this: (a) the entrainment relation is obtained by solving a series of equations in which the buoyancy flux F is constant. Hence, it is more suitable for buoyant jets in uniform ambient, and would give accurate result in such cases; (b) pockets of unstable regions giving rise to counter-gradient or reversible buoyancy flux that makes measurement of δ_g and θ_g difficult (see [32] for more details). Presence of reversible buoyancy flux disrupts the Reynolds stress correlation and contaminates the measurement of irreversible buoyancy flux. The effect becomes more apparent when the local Ri is high, thus the mismatch between the two approaches is pronounced in zone two. Because of this, the buoyancy term may influence the energy conversion term in the entrainment relation, giving rise to inaccurate physics. This can be fixed by segregating the reversible and the irreversible fluxes and ensuring only the later is taken into account.

4.4.2 Zone three

For the pure jet case, beyond $z/D \approx 20$ or zone three, the entrainment hypothesis and entrainment relation do not show any agreement. As we have discussed previously, this is because of the upper horizontal boundary's influence. The α values obtained from the entrainment relation and entrainment hypothesis can be reconciled by using appropriate boundary conditions in the formulation of ER that will impose necessary restrictions on it.

Lastly, in zone three of the buoyant jet, the entrainment relation does not capture the detrainment process even qualitatively. This is attributed to the inconsistency in the energy conversion term near the neutral layer because of the fluctuations in velocity components. The physical reasoning to that is the non-stationary nature of the field variables and its fluctuation in this region. To better understand this, Fig. 15 should be brought into the discussion. Here, the contributions from individual terms appearing in the entrainment relation for BJA is presented. For BJB also, the qualitative trends of the individual contributors to entrainment coefficient is the same and therefore not

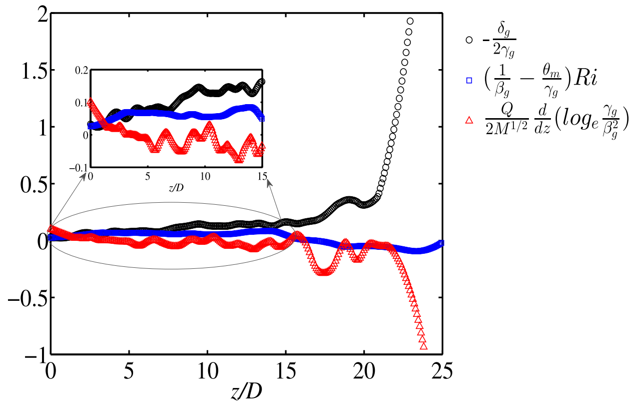

Fig. 15 Contributions from the different terms appearing in entrainment relation (Eq. 12b) for buoyant jet A as a function of axial distance. The entrainment coefficient is the algebraic sum of all the terms

Table 1 Experimental parameters

Parameter	Expression	Pure jet	BJA	BJB
Jet mean velocity	W_o	0.22	0.22	0.22
Reynolds number	$Re_o = \frac{\rho_j W_o D}{\mu}$	≈ 3100	≈ 3100	≈ 3100
Volume flux	$Q_o = W_o \frac{\pi D^2}{4}$	2.8×10^{-5}	2.8×10^{-5}	2.8×10^{-5}
Momentum flux	$M_o = Q_o W_o$	6.1×10^{-6}	6.1×10^{-6}	6.1×10^{-6}
Jet density	ρ_j	998	995.7	993.5
Bottom density in T2	ρ_b	998	1002.4	1006.2
Top density in T2	ρ_t	998	996.7	995.8
Ambient depth in T2	H	0.39	0.36	0.3
Buoyancy frequency	$N = \sqrt{-\frac{g}{\rho_o}\frac{\rho_t - \rho_b}{H}}$	-	0.4	0.6
Reduced gravity	$g' = \frac{g}{\rho_o}(\rho_b - \rho_j)$	-	0.066	0.124
Richardson number	$Ri = \left(\frac{\pi}{4}\right)^{0.5}\sqrt{\frac{g'D}{W_o^2}}$	-	0.12	0.17
Bifurcation parameter	$\sigma_0 = \left(\frac{M_0 N}{F_0}\right)^{0.75}$	-	1.24	1.01
Integral buoyancy	$B_o = g' \frac{\pi D^2}{4}$	-	8.38×10^{-6}	1.57×10^{-5}
Buoyancy flux	$F_o = g' Q_o$	-	1.84×10^{-6}	3.46×10^{-6}

All the quantities are in MKS units

presented. Figure 15 shows that the contributions from the buoyancy and similarity drift term is enough to capture the entrainment/detrainment process in this region. The contribution from the energy conversion term should be dropped, as it suffers from reversible fluxes and non-stationarity. Another reason for the mismatch could be attributed to the role of viscosity in this region, wherein, dissipation definitely plays a role that should be accounted either theoretically or empirically.

Table 2 Spatially averaged entrainment coefficient (α) for all the experimental cases in different zones using standard entrainment hypothesis (SEH) and entrainment relation (ER)

Case	α in zone one, SEH (ER)	α in zone two, SEH (ER)	α in zone three, SEH (ER)
Pure jet (α_{pj})	0.095 (0.081) ($0 \leq z/D < 10$)	0.098 (0.083) ($10 \leq z/D < 20$)	0.031 (0.091) ($z/D \geq 20$)
BJA (α_{bjA})	0.121 (0.131) ($0 \leq z/D < 10$)	0.135 (0.176) ($10 \leq z/D < 15$)	− 0.213 (0.312) ($z/D \geq 15$)
BJB (α_{bjB})	0.115 (0.139) ($0 \leq z/D < 7$)	0.151 (0.283) ($7 \leq z/D < 13$)	− 0.315 (0.318) ($z/D \geq 13$)

4.4.3 Final remarks

The above discussion provides a broad idea on how to reconcile the two methods of determining the entrainment coefficient. It is also observed that in all the three zones, the fluctuating quantities seem to be triggering the mismatch. Therefore, one common theme applicable to all the three zones would be to take into account the contributions from the mean flow alone and neglect the contributions from fluctuating flow field (see [26, 33]). Primarily though, a new entrainment relation is needed by solving Eqs. 2–5, but this time accounting for $N \neq 0s^{-1}$ and variation of buoyancy flux F with z. All these aspects need a closer inspection and this is an exercise that is left as a scope for future work.

5 Conclusions

The energetics and entrainment characteristics of pure and buoyant jets were studied experimentally with the help of simultaneous velocity and density fields. For calculating entrainment, two different approaches were employed; namely the standard entrainment hypothesis and the entrainment relation given by van Reeuwijk and Craske [1]. At first, the flux parameters, such as volume flux, Q, momentum flux, M, and buoyancy flux, F were found that helped in quantifying the characteristic velocity, w_m, width, d_m and buoyancy, b_m as a function of axial distance. We noticed that the variation in these quantities was very different for pure jet and buoyant jets, cementing the role of buoyancy force and stratification strength on the mean flow dynamics of buoyant jets.

The radial velocity contour maps provided a qualitative representation of the entrainment characteristics of pure and buoyant jets. Zone one showed patchy entrainment features, whereas zone two had more continuous entrainment features that clearly distinguished pure and buoyant jets. Finally in zone three, weak entrainment was seen for the pure jet while detrainment was seen for buoyant jets due to the presence of neutral buoyant layer. Subsequently, the entrainment coefficient, α, was quantified for the pure jet, buoyant jet with $N = 0.4\,\mathrm{s}^{-1}$ (or BJA) and $N = 0.6\,\mathrm{s}^{-1}$ (or BJB) using the standard entrainment hypothesis and entrainment relation. Based on the entrainment features and jet properties, for each of the three experimental cases, the entire axial distance was divided into three zones. In zone one, two and three, significant differences were seen, owing to the effect of buoyancy, wherein, in zone one and two, the $\alpha_{bj} > \alpha_{pj}$. In zone three, α_{pj} was very low for the pure jet whereas, $\alpha_{bj} < 0$ for buoyant jets due to detrainment process.

It was seen that α predicted using the entrainment hypothesis and entrainment relation agreed very well in zone one and two for the pure jet and zone one of BJA and BJB. In zone two of BJA and BJB there were discrepancies seen between the two approaches and it was appropriately discussed. Nevertheless, there was a reasonable match in the values of α for the pure jet case in zones one and two and for buoyant jets in zone one, using the two methods. However, zone three was the most critical where the entrainment relation did not match with the entrainment hypothesis. This was mainly attributed to the inaccurate representation of dissipation and energy conversion terms for buoyant jets and the upper horizontal boundary in the case of pure jet. Based on the experimental results, we proposed ways in which the energy-consistent entrainment relation given by van Reeuwijk and Craske [1] could be modified. We truly believe that the discussions provided in this paper could be very useful in coming up with a suitable entrainment relation for stably-stratified flows, especially in the far field region.

Acknowledgements Sridhar Balasubramanian is grateful for the funding support from Ministry of Earth Sciences (MoES) and Department of Science and Technology (DST). Partho Mukherjee and Harish Mirajkar acknowledge research scholarship from Ministry of Education, India.

References

1. van Reeuwijk M, Craske J (2015) Energy-consistent entrainment relations for jets and plumes. J Fluid Mech 782:333–355
2. Corrsin S (1943) Investigation of flow in an axially symmetrical heated jet of air. Wash, Wartime report
3. Davies POAL, Fisher MJ, Barratt MJ (1963) The characteristics of the turbulence in the mixing region of a round jet. J Fluid Mech 15(3):337–367
4. Crow SC, Champagne FH (1971) Orderly structure in jet turbulence. J Fluid Mech 48(3):547–591
5. Priestley CHB, Ball FK (1955) Continuous convection from an isolated source of heat. Q J R Meteorol Soc 81(348):144–157
6. Morton BR, Taylor GI, Turner JS (1956) Turbulent gravitational convection from maintained and instantaneous sources. Proc R Soc Lond Ser A Math Phys Sci 234(1196):1–23. https://doi.org/10.1098/rspa.1956.0011
7. Morton BR (1959) Forced plumes. J Fluid Mech 5(1):151–163
8. Wong DR, Wright SJ (1988) Submerged turbulent jets in stagnant linearly stratified fluids. J Hydraul Res 26(2):199–223
9. Turner JS (1986) Turbulent entrainment: the development of the entrainment assumption, and its application to geophysical flows. J Fluid Mech 173:431–471
10. Ellison TH, Turner JS (1959) Turbulent entrainment in stratified flows. J Fluid Mech 6(3):423–448
11. Princevac M, Fernando HJS, Whiteman CD (2005) Turbulent entrainment into natural gravity-driven flows. J Fluid Mech 533:259–268
12. Fischer HB, List EJ, Koh RCY, Imberger J, Brooks NH (1979) Chapter 9—turbulent jets and plumes. In: Mixing in inland and coastal waters. Academic Press, San Diego, pp 315–389. ISBN:978-0-08-051177-1
13. Bloomfield LJ, Kerr RC (2000) A theoretical model of a turbulent fountain. J Fluid Mech 424:197–216
14. Narasimha R, Diwan SS, Duvvuri S, Sreenivas KR, Bhat GS (2011) Laboratory simulations show diabatic heating drives cumulus-cloud evolution and entrainment. Proc Natl Acad Sci 108(39):16164–16169
15. Telford JW (1966) The Convective Mechanism in Clear Air. J Atmosp Sci 23(6):652–666
16. Papanicolaou PN, List EJ (1988) Investigations of round vertical turbulent buoyant jets. J Fluid Mech 195:341–391
17. Panchapakesan NR, Lumley JL (1993) Turbulence measurements in axisymmetric jets of air and helium. Part 1. Air jet. J Fluid Mech 246:197–223
18. Panchapakesan NR, Lumley JL (1993) Turbulence measurements in axisymmetric jets of air and helium. part 2. Helium jet. J Fluid Mech 246:225–247

19. Shabbir A, George WK (1994) Experiments on a round turbulent buoyant plume. J Fluid Mech 275:1–32
20. Duo X, Chen J (2012) Experimental study of stratified jet by simultaneous measurements of velocity and density fields. Exp Fluids 53(1):145–162
21. Mirajkar HN, Mukherjee P, Balasubramanian S (2020) Piv study of the dynamics of a forced plume in a stratified ambient. J Flow Visualiz Image Process 27:1
22. Talluru KM, Armfield S, Williamson N, Kirkpatrick MP, Milton-McGurk L (2021) Turbulence structure of neutral and negatively buoyant jets. J Fluid Mech 909:A14
23. Breda M, Buxton ORH (2018) Influence of coherent structures on the evolution of an axisymmetric turbulent jet. Phys Fluids 30(3):035109
24. Krug D, Chung D, Philip J, Marusic I (2017) Global and local aspects of entrainment in temporal plumes. J Fluid Mech 812:222–250
25. Pant CS, Bhattacharya A (2018) Evaluation of an energy consistent entrainment model for volumetrically forced jets using large eddy simulations. Phy Fluids 30(10):105107
26. Kaminski E, Tait S, Carazzo G (2005) Turbulent entrainment in jets with arbitrary buoyancy. J Fluid Mech 526:361–376
27. Oster G, Yamamoto M (1963) Density gradient techniques. Chem Rev 63(3):257–268
28. Mehta RD, Bradshaw P (1979) Design rules for small low speed wind tunnels. Aeronaut J (1968) 83(827):443–453
29. Adrian RJ (1991) Particle-imaging techniques for experimental fluid mechanics. Annu Rev Fluid Mech 23(1):261–304
30. Mirajkar HN, Balasubramanian S (2017) Effects of varying ambient stratification strengths on the dynamics of a turbulent buoyant plume. J Hydraul Eng 143(7):04017013
31. Matulka A, López P, Redondo JM, Tarquis A (2014) On the entrainment coefficient in a forced plume: quantitative effects of source parameters. Nonlinear Process Geophys 21(1):269–278
32. Peltier WR, Caulfield CP (2003) Mixing efficiency in stratified shear flows. Annu Rev Fluid Mech 35(1):135–167
33. Morton BR (1971) The choice of conservation equations for plume models. J Geophys Res (1896–1977) 76(30):7409–7416

Authors and Affiliations

Partho Mukherjee[1] · Harish N. Mirajkar[2] · Sridhar Balasubramanian[1,3]

✉ Sridhar Balasubramanian
sridharb@iitb.ac.in

1 Geophysical and Multiphase Flows Laboratory, Department of Mechanical Engineering, Indian Institute of Technology Bombay, Powai, Mumbai, Maharashtra 400076, India

2 Engineering Mechanics Unit, Jawaharlal Nehru Centre for Advanced Scientific Research, Jakkur, Bengaluru, Karnataka 560064, India

3 Interdisciplinary Program in Climate Studies, Indian Institute of Technology Bombay, Powai, Mumbai, Maharashtra 400076, India